

TENSOR-STRUCTURED PCG FOR FINITE DIFFERENCE SOLVER
OF DOMAIN PATTERNS IN FERROELECTRIC MATERIAL

VĚNCESLAV CHUMCHAL, Liberec, PAVEL MARTON, Liberec & Praha,
MARTIN PLEŠINGER, Liberec, MARTINA ŠIMŮNKOVÁ, Liberec

Abstract. This paper presents a case study of application of the preconditioned method of conjugate gradients (CG) on a problem with operator resembling the structure of sum of Kronecker products. In particular, we are solving the Poisson’s equation on a sample of homogeneous isotropic ferroelectric material of cuboid shape, where the Laplacian is discretized by finite difference. We present several preconditioners that fits the Kronecker structure and thus can be efficiently implemented and applied. Preconditioner based on the Moore–Penrose pseudoinverse is extremely efficient for this particular problem, and also applicable (if we are able to store the dense right-hand side of our problem). We briefly analyze the computational cost of the method and individual preconditioners, and illustrate effectiveness of the chosen one by numerical experiments.

Although we describe our method as *preconditioned CG with pseudoinverse-based preconditioner*, it can also be seen as *pseudoinverse-based direct solver with iterative refinement by CG iteration*.

This work is motivated by real application, the method was already implemented in C/C++ code FERROD02 and first results were published in Physical Review B 107(9) (2023), paper id 094102.

Keywords: conjugate gradients, preconditioner, tensor, tensor product, Kronecker product structure, Laplace operator, Poisson’s equation, ferroelectric domain structure

MSC 2020: 15A06, 15A30, 15A69, 65F08, 65F10, 65N06

1. INTRODUCTION

We are interested in the computation of the electric field induced by the given distribution of electric charge density ρ within a dielectric material. For this, we use Poisson’s equation

$$-\Delta v = \eta$$

which links electric potential and charge density (Δ is the Laplace operator). In particular, η represents the rescaled density of electrostatic charge ($\eta = \rho/\epsilon$, where

ϵ is the electric permittivity of the material, which is considered here homogeneous and scalar), v denotes the electric potential induced by ρ .

The Poisson's equation directly follows from the third Maxwell's equation ($\nabla \cdot \delta = \eta$), relation between electric induction δ and the target electric field ϵ ($\delta = \epsilon\epsilon$), and from the relation between electric potential v and electric field

$$\epsilon = -\nabla \cdot v.$$

The existence of the potential is provided by the second Maxwell's equation ($\nabla \times \epsilon = 0$) for the electrostatics. Once the potential v is recovered from Poisson's equation, the sought vector field — the electric field ϵ can then be easily obtained from v using the second equation. For more details about the electrostatic considerations, see [17] or, e.g., [5]. Also, it is fair to note here, that we do not follow the standard notation of the physical quantities to avoid possible collisions with also very standard mathematical notation later on.

The ultimate goal of a wider work than presented here is to contribute to understanding the so-called ferroelectric domain structures that emerge within the ferroelectric materials, which are utilized in a broad range of applications in actuation, sensing, and beyond. The domain structures are known to have a critical impact on material's properties, and at the same time, they are very difficult to determine experimentally, particularly for nano-size domains. Therefore, numerical simulations of domain structures is a necessary prerequisite for their understanding and control. An important aspect of these simulations is determining how these domains are influenced by charged defects/dopants within the ferroelectric materials. In this paper, however, we focus only on the numerical estimation of the electric potential v , i.e., on approximate solution of the discretized Poisson's equation.

1.1. Problem description and its discretization. Although our goal is to solve real-world-like, so three-dimensional (3D) problems, we start with simpler model problems that are only two-dimensional (2D). We are interested only in rectangular 2D or cuboid 3D domains. This choice is suitable from the computational point of view because it imposes Kronecker structure to the problem. However, it is also relevant from the practical, application point of view — we often deal with periodic boundary condition of the sample, where the cuboid can be seen as a single cell in larger periodic structure, which, e.g., opens door to Fourier approach.

On each pair of the opposite sides, or faces of the rectangle, or cuboid, respectively, there can be one of the following four types of boundary conditions (BC):

- Periodic BC (e.g., the electric potential on the left side of rectangle is the same as on the right side; it reflects periodicity of microscopic structure of the material);

- Dirichlet BC (which prescribes electric potential on the boundary);
- Neumann BC (which prescribes derivative of electric potential, i.e., the electric field over the boundary); or
- Mixed BC, in particular Dirichlet BC on one side (or face) and Neumann BC on the opposite.

Notice that for some combinations of boundary conditions — in particular periodic or Neumann in both (all three) directions — the Laplacian is not invertible, i.e., the solution is not unique, it is given up to a constant electric potential (notice, this does not affect its gradient and thus the electric field).

Due to the simple geometry, we consider the finite difference (FD) discretization. Since such discretization of the Laplace operator in two (or three) mutually orthogonal directions is trivial, the only two pieces of information we have in hands are: The discretized right-hand side η , i.e., a matrix $H \in \mathbb{R}^{n \times q}$ or its three-way analogue — a tensor $\mathcal{H} \in \mathbb{R}^{n \times q \times t}$, and the structure of BCs. We are looking for discretized electric potential v , i.e., an unknown matrix $U \in \mathbb{R}^{n \times q}$ or an unknown tensor $\mathcal{U} \in \mathbb{R}^{n \times q \times t}$.

1.2. Notation and structure of the work. Throughout the paper we try to keep the convention that vectors are denoted by lowercase italic letters, whereas matrices by uppercase italic letters, and tensors by uppercase calligraphic letters; entries of these objects are also denoted by lowercase italic letter, for example $(A)_{i,j} = a_{i,j}$, or $(A)_{i,j,k} = a_{i,j,k}$. In particular I and I_n denotes the identity matrix of suitable or given size. Further, 1 , 1_n , $1_{n,q}$, and $1_{n,q,t}$ denotes number one, vector of ones, matrix of ones, or tensor of ones of suitable or given size; similarly 0 , 0_n , $0_{n,q}$, and $0_{n,q,t}$. By \otimes we denote Kronecker product of matrices, by \odot Hadamard (entry-wise) product of matrices, by \times_ℓ the ℓ -mode matrix-tensor product. As usual, A^{-1} denotes inverse of A (if it exists), A^\dagger the Moore–Penrose pseudoinverse, and $A^{\ominus-1}$, $A^{\odot\dagger}$ their Hadamard (entry-wise) versions. By λ or $\lambda(A)$ we denote the eigenvalue of A , by λ_k or $\lambda_k(A)$ we denote the k th largest one (including multiplicities), and $\sigma(A)$ denotes the spectrum (set of all eigenvalues) of A . Finally $\|v\|_2$ stands for the Euclidean (i.e., two) norm of vector v and $\|A\|_F$ for the Frobenius norm of matrix A .

The text is organized as follows: After the introduction in Section 1, we recapitulate some basic concepts and notation related to the tensor manipulation in Section 2. Section 3 describes the basic properties and structure of linear algebraic system originated in discrete Laplacian. Section 4 discusses application of the preconditioned method of conjugate gradients. The obtained results are presented in Section 5. Section 6 concludes the paper.

2. BASIC TENSOR CONCEPTS AND NOTATION

We are dealing with 2D (in the simplified model), or later also 3D data arranged into regular grid of rectangular, or cuboid shape (thanks to the cuboid shape of the analyzed sample of material and regular finite difference discretization). These data can be naturally written in the form of a matrix, or its three-way analogy, respectively. We call the latter simply a *tensor* as it is usual in the matrix computations community. It would be useful here to introduce the tensor-related notation used throughout the text. All the concepts below can be found, e.g., in the review paper of Kolda and Bader [11] and in the references therein.

2.1. Vectorization. Let $U \in \mathbb{R}^{n \times q}$ be a matrix with columns u_j and entries $u_{i,j}$, where $i = 1, \dots, n$, $j = 1 \dots, q$. By *vectorization* we understand mapping of U to one long column-vector

$$\begin{aligned} \text{vec}(U) &= [u_1^\top, u_2^\top, \dots, u_q^\top]^\top \\ &= [[u_{1,1}, u_{2,1}, \dots, u_{n,1}], [u_{1,2}, u_{2,2}, \dots, u_{n,2}], \dots, [u_{1,q}, u_{2,q}, \dots, u_{n,q}]]^\top \in \mathbb{R}^{nq} \end{aligned}$$

that collects all the columns of U , one beneath other. Equivalently, $\text{vec}(U)$ contains all the entries $u_{i,j}$ of U sorted in the inverse lexicographical order w.r.t. their multiindices (i, j) ; see for example [27].

The equivalent formulation can be directly generalized for a tensor $\mathcal{U} \in \mathbb{R}^{n \times q \times t}$ with entries $u_{i,j,k}$ described by multiindices (i, j, k) , i.e.,

$$\begin{aligned} \text{vec}(\mathcal{U}) &= [[u_{1,1,1}, \dots, u_{n,1,1}], [u_{1,2,1}, \dots, u_{n,2,1}], \dots, [u_{1,q,1}, \dots, u_{n,q,1}], \\ &\quad [u_{1,1,2}, \dots, u_{n,1,2}], [u_{1,2,2}, \dots, u_{n,2,2}], \dots, [u_{1,q,2}, \dots, u_{n,q,2}], \\ &\quad \dots, \\ &\quad [u_{1,1,t}, \dots, u_{n,1,t}], [u_{1,2,t}, \dots, u_{n,2,t}], \dots, [u_{1,q,t}, \dots, u_{n,q,t}]]^\top \in \mathbb{R}^{nqt}. \end{aligned}$$

(The inner brackets are there only for better legibility.)

2.2. Matrix-tensor product (MT). First recall the *Kronecker product* of two matrices $A \in \mathbb{R}^{m \times n}$ and $B \in \mathbb{R}^{p \times q}$, i.e.,

$$B \otimes A = \begin{bmatrix} b_{1,1}A & b_{1,2}A & \dots & b_{1,q}A \\ b_{2,1}A & b_{2,2}A & \dots & b_{2,q}A \\ \vdots & \vdots & \ddots & \vdots \\ b_{p,1}A & b_{p,2}A & \dots & b_{p,q}A \end{bmatrix} \in \mathbb{R}^{(mp) \times (nq)}.$$

It has a lot of interesting properties (see [6] or [27]), and a lot of relations to the standard matrix summation and multiplication. If A_1 and A_2 are matrices of the

same dimensions, and also B_1 and B_2 , then

$$(2.1) \quad (B_1 + B_2) \otimes (A_1 + A_2) = (B_1 \otimes A_1) + (B_1 \otimes A_2) + (B_2 \otimes A_1) + (B_2 \otimes A_2).$$

On the other hand, if products A_1A_2 and B_1B_2 exist, then

$$(2.2) \quad (B_1B_2) \otimes (A_1A_2) = (B_1 \otimes A_1)(B_2 \otimes A_2).$$

It relates also to vectorization; if $A \in \mathbb{R}^{m \times n}$, $U \in \mathbb{R}^{n \times p}$, and $B \in \mathbb{R}^{p \times q}$, then

$$(2.3) \quad \text{vec}(AUB^T) = (B \otimes A) \text{vec}(U).$$

Notice that in AUB^T the matrix A multiplies columns of U whereas B multiplies rows of U (both treated as column-vectors). In terms of entries: columns of U are collections of entries $u_{i,j}$ with variable first index i and all the other indices (here only the second j) is fixed; similarly rows are collections of entries $u_{i,j}$ with variable second index j , whereas all the other indices (here only the first i) is fixed.

The entry-wise point of view allows us again to generalize several concepts to tensors. Any collection of all entries $u_{i,j,k}$ with one particular, let say ℓ th ($\ell \in \{1, 2, 3\}$) index variable (e.g., for $\ell = 1$, $i = 1, 2, \dots, n$) and all the other indices fixed (e.g., $(j, k) = (3, 7)$) is called the ℓ -mode fiber (in our case $(3, 7)$ th 1-mode fiber). The ℓ -mode matrix-tensor product $M \times_\ell \mathcal{U}$ is then multiplication of M with all the ℓ -mode fibres (treated as column-vectors). In our case where $A \in \mathbb{R}^{m \times n}$, $B \in \mathbb{R}^{p \times q}$, $C \in \mathbb{R}^{s \times t}$, and $\mathcal{U} \in \mathbb{R}^{n \times q \times t}$, we get

$$\begin{aligned} A \times_1 \mathcal{U} &\in \mathbb{R}^{m \times q \times t}, & \text{vec}(A \times_1 \mathcal{U}) &= (I_t \otimes I_q \otimes A) \text{vec}(\mathcal{U}), \\ B \times_2 \mathcal{U} &\in \mathbb{R}^{n \times p \times t}, & \text{vec}(B \times_2 \mathcal{U}) &= (I_t \otimes B \otimes I_n) \text{vec}(\mathcal{U}), \\ C \times_3 \mathcal{U} &\in \mathbb{R}^{n \times q \times s}, & \text{vec}(C \times_3 \mathcal{U}) &= (C \otimes I_q \otimes I_n) \text{vec}(\mathcal{U}). \end{aligned}$$

Multiplication of a tensor by two matrices in two different modes is independent on the order of individual operations (which follows directly from the associativity of matrix multiplication). Therefore, we simplify the notation a bit in the case of *general linear transformation* of the tensor

$$(A, B, C | \mathcal{U}) = A \times_1 (B \times_2 (C \times_3 \mathcal{U})) \in \mathbb{R}^{m \times p \times s}.$$

Similarly as before,

$$\text{vec}((A, B, C | \mathcal{U})) = (C \otimes B \otimes A) \text{vec}(\mathcal{U}).$$

For deeper insight into tensor manipulation we recommend to study [11].

Finally, notice that in our case the transforming matrices A , B , and C will always be square, symmetric, and positive semi-definite.

3. DESCRIPTION OF THE ALGEBRAIC SYSTEM

As already mentioned, we are focused on solving the discretized Poisson's equation

$$-\Delta v = \eta;$$

see [4]. We use regular 2D or 3D finite difference discretization with the mesh oriented in accordance with the sample of material. We moreover assume, for simplicity, that the material is homogenous and isotropous, i.e., the material coefficients does not change along the discretization and in different orientations. Therefore we have very simple discretization of the (minus) Laplace operator.

3.1. Discretization of 1D Laplace operator. Recall that in one-dimensional (1D) case, the finite difference discretization of the *minus* Laplacian takes exceptionally simple form

$$(3.1) \quad L_n(\alpha, \beta, \gamma) = \begin{bmatrix} \alpha & -1 & & & & & \gamma \\ -1 & 2 & -1 & & & & \\ & -1 & 2 & \ddots & & & \\ & & \ddots & \ddots & -1 & & \\ & & & -1 & 2 & -1 & \\ \gamma & & & & -1 & \beta & \end{bmatrix} \in \mathbb{R}^{n \times n}, \quad n \geq 3,$$

see, e.g., [6], [29]. The matrix is obviously symmetric $L_n(\alpha, \beta, \gamma) = (L_n(\alpha, \beta, \gamma))^T$. Values of entries in its corners depend on BCs, in particular:

- Periodic BC enforces $(\alpha, \beta, \gamma) = (2, 2, -1)$;
- Dirichlet BC enforces $(\alpha, \beta, \gamma) = (2, 2, 0)$;
- Neumann BC enforces $(\alpha, \beta, \gamma) = (1, 1, 0)$; and
- Mixed BC enforces $(\alpha, \beta, \gamma) = (2, 1, 0)$ or $(1, 2, 0)$.

If it is not so important, then we will denote the matrix simply L_n or even L . On the other hand, if we need to distinguish the particular BC/matrix structure, we use

$$L_{n,P} = L_n(2, 2, -1), \quad L_{n,D} = L_n(2, 2, 0), \quad L_{n,N} = L_n(1, 1, 0), \\ L_{n,DN} = L_n(2, 1, 0), \quad \text{and} \quad L_{n,ND} = L_n(1, 2, 0).$$

Notice, that the BC affects in general also the right-hand side of the algebraic systems; see Section 3.4.

3.2. Spectral properties of L_n matrices. Here we briefly mention the basic spectral properties (eigenvalues and eigenpairs) of matrices L_n . We listed them without proofs, but these results are commonly known and can be easily verified (simply by multiplication the matrices by respective vectors and employing basic trigonometry); see for example [10].

Lemma 3.1 (Spectral properties of $L_{n,P}$). *Let $n \in \mathbb{N}$, $n \geq 3$. Consider $\ell \in \mathbb{N}$ such that either $n = 2\ell - 1$ or $n = 2\ell$. Then*

$$\lambda_1 = 0, \quad \lambda_{2k} = \lambda_{2k+1} = 2 - 2 \cos\left(\frac{2k\pi}{n}\right), \quad k = 1, \dots, \ell - 1, \quad \lambda_{2\ell} = 4,$$

represent the eigenvalues and

$$\begin{aligned} v_1 &= [1, 1, \dots, 1]^\top, \\ v_{2k} &= \left[\cos\left(\frac{2jk\pi}{n}\right) \right]_{j=1}^n, \quad v_{2k+1} = \left[\sin\left(\frac{2jk\pi}{n}\right) \right]_{j=1}^n, \quad k = 1, \dots, \ell - 1, \\ v_{2\ell} &= [1, -1, \dots, 1, -1]^\top. \end{aligned}$$

the eigenvectors of $L_{n,P}$ (except of the last pair in the odd n case).

Lemma 3.2 (Spectral properties of $L_{n,D}$). *Let $n \in \mathbb{N}$, $n \geq 3$. Then*

$$\lambda_k = 2 - 2 \cos\left(\frac{k\pi}{n+1}\right), \quad v_k = \left[\sin\left(\frac{jk\pi}{n+1}\right) \right]_{j=1}^n, \quad k = 1, \dots, n,$$

represent the eigenvalues and the eigenvectors of $L_{n,D}$.

Lemma 3.3 (Spectral properties of $L_{n,N}$). *Let $n \in \mathbb{N}$, $n \geq 3$. Then*

$$\lambda_k = 2 - 2 \cos\left(\frac{(k-1)\pi}{n}\right), \quad v_k = \left[\cos\left(\frac{(j-\frac{1}{2})(k-1)\pi}{n}\right) \right]_{j=1}^n, \quad k = 1, \dots, n,$$

represent the eigenvalues and the eigenvectors of $L_{n,N}$.

Lemma 3.4 (Spectral properties of $L_{n,DN}$ and $L_{n,ND}$). *Let $n \in \mathbb{N}$, $n \geq 3$. Then*

$$\lambda_k = 2 - 2 \cos\left(\frac{(2k-1)\pi}{2n+1}\right), \quad v_k = \left\{ \begin{array}{l} \left[\sin\left(\frac{j(2k-1)\pi}{2n+1} - k\pi\right) \right]_{j=1}^n \\ \left[\cos\left(\frac{j(2k-1)\pi}{2n+1} - \frac{(2k-1)\pi}{2(2n+1)}\right) \right]_{j=1}^n \end{array} \right\},$$

$k = 1, \dots, n$, represent the eigenvalues and the eigenvectors of $L_{n,DN}$ and $L_{n,ND}$, respectively.

The goal of this list is to point out several things. First, we see, that all the spectral information of all the matrices is available in analytical form. Second, we see, that essentially all the eigenvalues are of the form $2 - 2 \cos(f(j)\pi/g(n))$, where $f(x)$ and $g(x)$ are linear functions, $f(x)$ is nonnegative and $g(x)$ positive on the

respective domain and $f(j) < g(n)$. Thus, all the eigenvalues of all the matrices are nonnegative from interval $[0, 4]$. Third, actually most of the eigenvalues are positive — there are only two exceptions

$$\lambda_1(L_{n,\text{P}}) = \lambda_1(L_{n,\text{N}}) = 0.$$

Consequently, matrices $L_{n,\text{D}}$, $L_{n,\text{DN}}$, $L_{n,\text{ND}}$ are always symmetric positive definite, whereas $L_{n,\text{P}}$ and $L_{n,\text{N}}$ are always only symmetric positive semi-definite, i.e., not invertible, $\det(L_{n,\text{P}}) = \det(L_{n,\text{N}}) = 0$. Finally, notice that matrices $L_{n,\text{DN}}$ and $L_{n,\text{ND}}$ in Lemma 3.4 are essentially the same, just upside-down & left-to-right rearranged. Therefore, also their eigenvectors are essentially the same (only upside-down rearranged, i.e., reindexed by $j \mapsto n + 1 - j$ and after few goniometric manipulations multiplied by -1).

3.3. Discretization of 2D & 3D Laplacians and their spectra. In the 1D case, our equation $-\Delta v = \eta$ is by *finite differences* (FD) projected to the discrete space as

$$-\Delta_{\text{FD}}(u) \equiv L_n u = h.$$

In 2D and 3D cases is situation very similar. Thanks to the discretization independent in individual directions and thanks to simple scalar homogenous properties of the material, we get

$$(3.2) \quad -\Delta_{\text{FD}}(U) \equiv L_n U + U L_q^{\text{T}} = H, \quad -\Delta_{\text{FD}}(\mathcal{U}) \equiv L_n \times_1 \mathcal{U} + L_q \times_2 \mathcal{U} + L_t \times_3 \mathcal{U} = \mathcal{H},$$

respectively; see, e.g., [6], [29]. By vectorization of these equations we get them in the standard form with single matrix, vector of unknowns and the right-hand side vector

$$(3.3) \quad \begin{aligned} & \overbrace{\left((I_q \otimes L_n) + (L_q \otimes I_n) \right)}^{L_{2\text{D}} \in \mathbb{R}^{(nq) \times (nq)}} \text{vec}(U) = \text{vec}(H), \\ & \underbrace{\left((I_t \otimes I_q \otimes L_n) + (I_t \otimes L_q \otimes I_n) + (L_t \otimes I_q \otimes I_n) \right)}_{L_{3\text{D}} \in \mathbb{R}^{(nqt) \times (nqt)}} \text{vec}(\mathcal{U}) = \text{vec}(\mathcal{H}). \end{aligned}$$

It is clear that these matrices are unnecessarily big, since all the useful information is carried only by the two, or three bits of information — the individual L_ℓ matrices. These big matrices are cannot be used for practical computation, but they can provide us a lot of useful information.

Since our matrix L_ℓ is symmetric, we can always write it in the form of spectral decomposition, i.e., as a product

$$(3.4) \quad L_\ell = V_\ell \Lambda_\ell V_\ell^{-1}.$$

Here Λ_ℓ is a diagonal matrix with diagonal entries equal to eigenvalues of L_ℓ , and V_ℓ is an invertible matrix with columns equal to eigenvector of L_ℓ (both given by Lemmas 3.1–3.4; notice that the eigenvectors are not normalized there). Employing (2.2), we get

$$(3.5) \quad \begin{aligned} L_{2D} &= \left((V_q V_q^{-1} \otimes V_n \Lambda_n V_n^{-1}) + (V_q \Lambda_q V_q^{-1} \otimes V_n V_n^{-1}) \right) \\ &= (V_q \otimes V_n) \left((I_q \otimes \Lambda_n) + (\Lambda_q \otimes I_n) \right) (V_q \otimes V_n)^{-1}, \end{aligned}$$

which is the spectral decomposition, and thus

$$\sigma(L_{2D}) = \{ \lambda_i(L_n) + \lambda_j(L_q) : i = 1, \dots, n, j = 1, \dots, q \}$$

is the spectrum of the discretized 2D minus Laplacian. Similarly,

$$\sigma(L_{3D}) = \{ \lambda_i(L_n) + \lambda_j(L_q) + \lambda_k(L_t) : i = 1, \dots, n, j = 1, \dots, q, k = 1, \dots, t \}$$

is the spectrum of the discretized 3D minus Laplacian.

Finally, we see that the big matrices L_{2D} and L_{3D} in (3.3) are always symmetric positive semi-definite. Moreover, they are invertible (and thus positive definite and thus (3.2) uniquely solvable) if and only if at least one of the matrices L_ℓ is invertible.

3.4. Modifications of the right-hand side enforced by BCs. Since the solving process of $\Delta v = \eta$ starts with the discretized right-hand side (obtained from the outside) and the sets of BCs, we need to ensure the compatibility of these two pieces of information. In particular the BCs will govern the structure of right-hand side. It will be done in a very standard way, thus we do only a few comments.

3.4.1. Orthogonality to null-space. First, recall that discretized 1D Laplacians $L_{n,P}$ and $L_{n,N}$ are singular, both with simple zero eigenvalue. Similarly, discretized 2D and 3D Laplacians (3.3) assembled only from $L_{n,P}$'s or $L_{n,N}$'s are singular with simple zero eigenvalue. In all these cases, the corresponding eigenvector, i.e., the vector in null-space of such discretized Laplacian is

$$\mathbf{1}_\ell = [1, 1, \dots, 1]^T \in \mathbb{R}^\ell$$

of suitable length ℓ . Thus, the discretized right-hand side $H \in \mathbb{R}^{n \times q}$, or $\mathcal{H} \in \mathbb{R}^{n \times q \times t}$ satisfies

$$\begin{aligned} \mathbf{1}_{nq} \perp \text{vec}(H) &\iff \mathbf{1}_n^\top H \mathbf{1}_q = 0, \\ \mathbf{1}_{nqt} \perp \text{vec}(\mathcal{H}) &\iff (\mathbf{1}_n^\top, \mathbf{1}_q^\top, \mathbf{1}_t^\top | \mathcal{H}) = 0. \end{aligned}$$

If it is not the case (in particular due to the rounding errors in the software that provides us the right-hand side; but also during the computation, see Remark 4.1; in principal also in the case, when the right-hand side is somehow measured), it is suitable to project-out data in the direction of vector $\mathbf{1}$, i.e., to do a modification of the form

$$(3.6) \quad H \mapsto H - \mathbf{1}_{n,q} \cdot \frac{1}{nq} \cdot \sum_{i=1}^n \sum_{j=1}^q h_{i,j}, \quad \mathcal{H} \mapsto \mathcal{H} - \mathbf{1}_{n,q,t} \cdot \frac{1}{nqt} \cdot \sum_{i=1}^n \sum_{j=1}^q \sum_{k=1}^t h_{i,j,k},$$

i.e., to center the data.

3.4.2. Dirichlet and Neumann BCs update. If a Dirichlet or a Neumann BC is prescribed, then there is given particular value of electric potential or its derivative (electric field), constant on the whole side or face. We demonstrate the right-hand side update for simplicity only on the 1D case $L_n u = h$.

Consider the Dirichlet BC at the “beginning” of 1D sample and let the prescribed value of the electric potential be u_B . Technically the prescription is done such that

$$\left[\begin{array}{c|ccc} -1 & 2 & -1 & \\ & -1 & 2 & -1 \\ & & \ddots & \ddots \\ & & & \ddots \end{array} \right] \left[\begin{array}{c} u_B \\ u_1 \\ u_2 \\ \vdots \end{array} \right] = \left[\begin{array}{c} h_1 \\ h_2 \\ \vdots \end{array} \right],$$

which can be equivalently written as

$$L_{n,D} u = h + i_1 u_B,$$

where i_ℓ denotes the ℓ th column of I . (Similar update $i_n u_E$ will be originated also from the value prescribed “end”.)

Neumann BC at the “beginning” of 1D sample prescribes the value of the electric field, i.e., the derivative of electric potential over the boundary. Let it be e_B . Technically

$$\left[\begin{array}{c|ccc} -1 & 2 & -1 & \\ & -1 & 2 & -1 \\ & & \ddots & \ddots \\ & & & \ddots \end{array} \right] \left[\begin{array}{c} u_1 + e_B \\ u_1 \\ u_2 \\ \vdots \end{array} \right] = \left[\begin{array}{c|ccc} -1 & 1 & -1 & \\ & -1 & 2 & -1 \\ & & \ddots & \ddots \\ & & & \ddots \end{array} \right] \left[\begin{array}{c} e_B \\ u_1 \\ u_2 \\ \vdots \end{array} \right] = \left[\begin{array}{c} h_1 \\ h_2 \\ \vdots \end{array} \right],$$

which can be equivalently written as

$$L_{n,\mathbf{N}} u = h + i_1 e_{\mathbf{B}}.$$

(Similar update $i_n e_{\mathbf{E}}$ will be originated also from the value prescribed “end”.)

These two BCs can be easily combined in the 1D case, leading to $L_{n,\mathbf{DN}}$ or $L_{n,\mathbf{ND}}$ matrix and mixed updates $(i_1 u_{\mathbf{B}} + i_n e_{\mathbf{E}})$ or $(i_1 e_{\mathbf{B}} + i_n u_{\mathbf{E}})$ of the right-hand side.

4. PRECONDITIONED METHOD OF CONJUGATE GRADIENTS

Since the discretized Laplacians L_n and in particular (3.3) are either symmetric positive definite, or symmetric positive semi-definite, but compatible, i.e., with the right-hand side orthogonal to the null-space of the operator (see Section 3.4.1), we can use the method of conjugate gradients (CG), in particular its preconditioned variant (PCG) for solving such system; see [9]; see also [13] for deeper understanding and wider context, [18] for computational aspects, [14] for preconditioning of CG, and [20], [19] for error estimation and stopping criterions.

Recall that the preconditioner is a linear operator. After discretization of the problem, preconditioner represented by matrix M is applied on both sides of $L_n u = h$ (in the 1D case), yielding the preconditioned system $M L_n u = M h$. If M is symmetric and positive definite, then there exists matrix $M^{\frac{1}{2}}$ so that $M = M^{\frac{1}{2}} M^{\frac{1}{2}}$. The preconditioned system can be then further rearranged to $(M^{\frac{1}{2}} L_n M^{\frac{1}{2}})(M^{-\frac{1}{2}} u) = (M^{-\frac{1}{2}} h)$ with symmetric matrix $M^{\frac{1}{2}} L_n M^{\frac{1}{2}}$ that is of the same definiteness as L_n . Consequently, the standard CG can be applied to the latest system; however it approximates $M^{-\frac{1}{2}} u$ vector. After a few manipulations to express u , we get the usual PCG algorithm.

4.1. PCG algorithm. Since the PCG is a very standard algorithm, we explicitly mention only its variant for our 3D problem; see Algorithm 1. To get its 2D variant it is sufficient to replace all the three-way tensors by matrices — formally replace all the calligraphic letters \mathcal{H} , \mathcal{U}_s , \mathcal{W}_s , \mathcal{R}_s , \mathcal{Z}_s , and \mathcal{P}_s , by its uppercase italic counterparts.

Remark 4.1 (Orthogonality to null-space). *Consider the discretized Laplacian which is singular (in 1D case $L_{n,\mathbf{P}}$, see Lemma 3.1, or $L_{n,\mathbf{N}}$, see Lemma 3.3). Its null-space is one-dimensional, spanned by $\mathbf{1}_n = [1, 1, \dots, 1]^T$ in 1D, $\mathbf{1}_{n,q}$ in 2D, and $\mathbf{1}_{n,q,t}$ in 3D case.*

If the right-hand side \mathcal{H} is orthogonal to the null-space (see Section 3.4.1), and also the initial guess \mathcal{U}_0 (notice that the initial guess is often zero, $\mathcal{U}_0 = 0_{n,q,t}$), then the whole CG (PCG with \mathfrak{M} being identity) is orthogonal to this null-space. In particular vectors, \mathcal{U}_s , \mathcal{W}_s , \mathcal{R}_s , and \mathcal{P}_s are orthogonal to $\mathbf{1}_{n,q,t}$. In the finite precision arithmetic, a nonzero projection into the null-space may be generated due

Algorithm 1 Preconditioned CG for discretized 3D Poisson's equation

```
1: Input  $\Delta_{\text{FD}}, \mathcal{H}, \mathfrak{M}, \mathcal{U}_0$       {Laplacian, right-hand side, preconditioner, initial
    guess}
2:  $s \leftarrow 0$ 
3:  $\mathcal{W}_0 \leftarrow -\Delta_{\text{FD}}(\mathcal{U}_0)$       {application of discretized minus Laplacian}
4:  $\mathcal{R}_0 \leftarrow \mathcal{H} - \mathcal{W}_0$           {initial residuum}
5:  $\mathcal{Z}_0 \leftarrow \mathfrak{M}(\mathcal{R}_0)$           {application of preconditioner}
6:  $\rho_0 \leftarrow \langle \mathcal{R}_0, \mathcal{Z}_0 \rangle$ 
7:  $\mathcal{P}_0 \leftarrow \mathcal{Z}_0$ 
8: Repeat
9:    $s \leftarrow s + 1$ 
10:   $\mathcal{W}_s \leftarrow -\Delta_{\text{FD}}(\mathcal{P}_{s-1})$   {application of discretized minus Laplacian}
11:   $\alpha_s \leftarrow \rho_{s-1} / \langle \mathcal{W}_s, \mathcal{P}_{s-1} \rangle$ 
12:   $\mathcal{U}_s \leftarrow \mathcal{U}_{s-1} + \alpha_s \mathcal{P}_{s-1}$   {update of solution approximation}
13:   $\mathcal{R}_s \leftarrow \mathcal{R}_{s-1} - \alpha_s \mathcal{W}_s$   {update of residuum}
14:   $\mathcal{Z}_s \leftarrow \mathfrak{M}(\mathcal{R}_s)$           {application of preconditioner}
15:   $\rho_s \leftarrow \langle \mathcal{R}_s, \mathcal{Z}_s \rangle$ 
16:   $\beta_s \leftarrow \rho_s / \rho_{s-1}$ 
17:   $\mathcal{P}_s \leftarrow \mathcal{Z}_s + \beta_s \mathcal{P}_{s-1}$ 
18: Until stopping criterion match
19: Output  $\mathcal{U}_{\text{PCG}} \leftarrow \mathcal{U}_s$       {PCG approximation of  $\mathcal{U}$ }
```

to rounding errors. Therefore, it is suitable to center the data; see (3.6). It seems to be sufficient to center only one of the four quantities, once per iteration.

In the case of general PCG, the preconditioner \mathfrak{M} may generate nonzero projection of \mathcal{Z}_s into the null-space and thus affect the whole algorithm. Therefore, it is suitable to center \mathcal{Z}_s .

Remark 4.2 (Stopping criterion). *Since this work is rather a case study about behavior the PCG with different preconditioners when applied on our problem, we do not elaborate the stopping criterion. Actually, we stop simply at maximal number of iterations. This number is determined experimentally for each problem and preconditioner, so that the true residual decreases sufficiently. This choice seems to be, however, applicable even in our final practical C/C++ implementation.*

The best option for stopping is robust estimation of A-norm of error; see [20] and in particular paper [19].

4.2. Computational cost of PCG. The PCG algorithm consists of several typical subroutines. Some of them needs to be explored in details. We start from the simplest:

- **Saxpy type subroutine** (lines 4, 12, 13, and 17) that consists of simple entry-wise operations with matrices or three-way tensors. The cost of one saxpy is about $O(2nqt)$ of elementary operations; in the 2D case $t = 1$.
- **Inner product** (lines 6, 11, and 15) that can be for matrices and three-way tensors defined by employing the vectorization, e.g.,

$$\langle R, Z \rangle = \langle \text{vec}(R), \text{vec}(Z) \rangle = \sum_{i=1}^n \sum_{j=1}^q r_{i,j} \cdot z_{i,j},$$

$$\langle \mathcal{R}, \mathcal{Z} \rangle = \langle \text{vec}(\mathcal{R}), \text{vec}(\mathcal{Z}) \rangle = \sum_{i=1}^n \sum_{j=1}^q \sum_{k=1}^t r_{i,j,k} \cdot z_{i,j,k}.$$

The cost of one inner product is about $O(2nqt)$ of elementary operations.

- **Application of minus Laplacian** (lines 3 and 10) that needs to be broken down to operations with the small 1D Laplacian matrices L_ℓ , e.g.,

$$W = -\Delta_{\text{FD}}(P) = L_n P + P L_q^T, \quad \mathcal{W} = -\Delta_{\text{FD}}(\mathcal{P}) = L_n \times_1 \mathcal{P} + L_q \times_2 \mathcal{P} + L_t \times_3 \mathcal{P},$$

with entries

$$w_{\zeta,\xi} = \sum_{i=1}^n (L_n)_{\zeta,i} \cdot p_{i,\xi} + \sum_{j=1}^q (L_q)_{\xi,j} \cdot p_{\zeta,j},$$

$$w_{\zeta,\xi,\nu} = \sum_{i=1}^n (L_n)_{\zeta,i} \cdot p_{i,\xi,\nu} + \sum_{j=1}^q (L_q)_{\xi,j} \cdot p_{\zeta,j,\nu} + \sum_{k=1}^t (L_t)_{\nu,k} \cdot p_{\zeta,\xi,k}.$$

The cost of one application of a general operator with this structure is about $O(2nq(n+q))$ and $O(2nqt(n+q+t))$, in 2D and 3D case, respectively. Here, however, the sparsity of L_ℓ matrices can (and needs to) be utilized in the practical implementation — since they have only three nonzero entries per row, the cost can be reduced to about $O(12nqt)$ and $O(18nqt)$, respectively.

- **Application of preconditioner** (lines 5 and 14) depends on the particular choice of preconditioner. Clearly, it is useful to look for such one, which does not increase the computational cost significantly.

The overall cost of our PCG implementation is in Table 1. The cost of preconditioning is not taken into the account. In the case of singular discretized Laplacian, each data centering (see Section 3.4.1 and Remark 4.1) increases the cost by $3nqt$ elementary operations — typically once per iteration. Similarly, the evaluation of stopping criterion (see Remark 4.2) may costs some further operations.

4.3. Preconditioner. Typically we are looking for such preconditioner, that somehow resembles the tensor (or matrix) structure of the algorithm, which does not

TABLE 1. Cost (measured by number of elementary operations) of matrix (2D) and tensor (3D) variants of PCG with Kronecker-structured operator with sparse matrices (three nonzeros per row); see Algorithm 1. Preconditioner is not included.

App. of Laplacian	Initialization (lines 2–7)		Iteration (lines 9–17)	
	Full	Sparse	Full	Sparse
Cost of 2D variant	$2nq(n+q+2)$	$16nq$	$2nq(n+q+5)$	$22nq$
Cost of 3D variant	$2nqt(n+q+t+2)$	$22nqt$	$2nqt(n+q+t+5)$	$28nqt$

increase the computational cost, and which, of course, speed up the convergence. Notice that relevant is the computational cost per iteration, not the cost of the preparatory work, that is done once, at the beginning of PCG. We have experimented with only few families of preconditioners:

- Several steps of stationary iterative method — because of symmetry of L_ℓ s, we decided to use Jacobi-like method (standard and weighted Jacobi).
- Approximate inverse of $(-\Delta_{\text{FD}})$ of low-Kronecker-rank (Kronecker-rank denotes the number of summands when the matrix is expressed as in (3.3); notice that $(-\Delta_{\text{FD}})$ is always of low-Kronecker-rank, equal to two or three, in the 2D and 3D case, respectively).
- Moore–Penrose pseudoinverse of $(-\Delta_{\text{FD}})$.

Implementation of a preconditioner into PCG consists of two subroutines: The first one prepares all the parts of the preconditioner that can be computed only once, in beforehand, while initialization of PCG. The other one is the application of the precomputed preconditioner on the updated residual (see lines 5 and 14 of Algorithm 1).

4.3.1. *Preconditioning by several steps of Jacobi-like method.* Consider parametrized splitting of matrix $A \in \mathbb{R}^{n \times n}$ in the form

$$A = D_\omega(A) + O_\omega(A), \quad \text{where} \quad D_\omega(A) = D \cdot \omega, \quad O_\omega(A) = O + D \cdot (1 - \omega),$$

and where $D = \text{diag}(a_{1,1}, a_{2,2}, \dots, a_{n,n}) \in \mathbb{R}^{n \times n}$ contains the diagonal entries of A , $O = A - D$ the off-diagonal entries, and $\omega \in [1, \infty)$ is the real weighting parameter. The associated stationary method applied on $Ax = b$ iterates as

$$(4.1) \quad x_j = (D_\omega(A))^{-1}(b - O_\omega(A)x_{j-1}).$$

If $\omega = 1$, the splitting and the associated method is called Jacobi, if $\omega > 1$, it is called weighted Jacobi.

Matrix $D_\omega(A)$ is diagonal, thus its inverse is easy to compute — just invert all the diagonal entries. If we handle its diagonal as a vector

$$\widehat{d}_\omega = \begin{bmatrix} a_{1,1} \\ a_{2,2} \\ \vdots \\ a_{n,n} \end{bmatrix} \cdot \omega \in \mathbb{R}^n \quad \text{and denote} \quad f_j = b - O_\omega(A)x_{j-1} \in \mathbb{R}^n,$$

then we can (4.1) rewrite as

$$(4.2) \quad x_j = (\widehat{d}_\omega)^{\circ-1} \odot f_j.$$

where \circ^{-1} denotes the *entry-wise inverse* also called *Hadamard inverse* of the vector, and \odot the *entry-wise* a.k.a. *Hadamard product*.

For Kronecker-structured matrix such as in (3.3), e.g.,

$$L_{2D} = (I_q \otimes L_n) + (L_q \otimes I_n)$$

in the 2D case, it is easy to see (using property (2.1)) that the splitting takes the same form, i.e.,

$$(4.3) \quad \begin{aligned} D_\omega(L_{2D}) &= (I_q \otimes D_\omega(L_n)) + (D_\omega(L_q) \otimes I_n), \\ O_\omega(L_{2D}) &= (I_q \otimes O_\omega(L_n)) + (O_\omega(L_q) \otimes I_n). \end{aligned}$$

Iteration (4.1) requires inverse of diagonal matrix $D_\omega(L_{2D})$, which can be again realized as in (4.2), by Hadamard inverse of

$$(4.4) \quad \widehat{D}_\omega = \begin{bmatrix} (L_n)_{1,1} + (L_q)_{1,1} & (L_n)_{1,1} + (L_q)_{2,2} & \cdots & (L_n)_{1,1} + (L_q)_{q,q} \\ (L_n)_{2,2} + (L_q)_{1,1} & (L_n)_{2,2} + (L_q)_{2,2} & \cdots & (L_n)_{2,2} + (L_q)_{q,q} \\ \vdots & \vdots & \ddots & \vdots \\ (L_n)_{n,n} + (L_q)_{1,1} & (L_n)_{n,n} + (L_q)_{2,2} & \cdots & (L_n)_{n,n} + (L_q)_{q,q} \end{bmatrix} \cdot \omega$$

and then by Hadamard product. To summarize, the only parts that needs to be precomputed are: Matrices $O_\omega(L_n)$, $O_\omega(L_q)$, and $(\widehat{D}_\omega)^{\circ-1}$ in the 2D case; matrices $O_\omega(L_n)$, $O_\omega(L_q)$, $O_\omega(L_t)$, and tensor $(\widehat{D}_\omega)^{\circ-1}$ in the 3D case.

For preconditioning CG we use p steps of this stationary method. It is applied on the problem with the updated residual on the right-hand side (see lines 5 and 14 of Algorithm 1) and with initial guess $x_0 = 0$. See Algorithm 2 for implementation for the 2D case and Algorithm 3 for the 3D case.

Algorithm 2 Application of preconditioner $Z_s \leftarrow \mathfrak{M}_{\text{Jacobi}(p,\omega)}(R_s)$, 2D case

1: **Precomputed** $O_\omega(L_n), O_\omega(L_q), (\widehat{D}_\omega)^{\odot -1}$
2: **Input** R_s {updated residual}
3: $X_0 = 0_{n,q}$
4: **For** $j \leftarrow 1, 2, \dots, p$
5: $F_j \leftarrow R_s - (O_\omega(L_n)X_{j-1} + X_{j-1}(O_\omega(L_q)))^\top$
6: $X_j \leftarrow (\widehat{D}_\omega)^{\odot -1} \odot F_j$
7: **End for**
8: **Output** $Z_s \leftarrow X_p$ {preconditioned residual}

Algorithm 3 Application of preconditioner $Z_s \leftarrow \mathfrak{M}_{\text{Jacobi}(p,\omega)}(\mathcal{R}_s)$, 3D case

1: **Precomputed** $O_\omega(L_n), O_\omega(L_q), O_\omega(L_t), (\widehat{D}_\omega)^{\odot -1}$
2: **Input** \mathcal{R}_s {updated residual}
3: $\mathcal{X}_0 = 0_{n,q,t}$
4: **For** $j \leftarrow 1, 2, \dots, p$
5: $\mathcal{F}_j \leftarrow \mathcal{R}_s - (O_\omega(L_n) \times_1 \mathcal{X}_{j-1} + O_\omega(L_q) \times_2 \mathcal{X}_{j-1} + O_\omega(L_t) \times_3 \mathcal{X}_{j-1})$
6: $\mathcal{X}_j \leftarrow (\widehat{D}_\omega)^{\odot -1} \odot \mathcal{F}_j$
7: **End for**
8: **Output** $Z_s \leftarrow \mathcal{X}_p$ {preconditioned residual}

4.3.2. *Preconditioning by a low-Kronecker-rank approximation of the inverse.* Recall that (3.2) can be rewritten as standard system (3.3) with matrix $((I_q \otimes L_n) + (L_q \otimes I_n))$. We would like to approximate its inverse, or generalized inverse (see [1]) since the original matrix may be singular, by a low Kronecker-rank matrix. In particular

$$L_{2D}^\dagger = \left((I_q \otimes L_n) + (L_q \otimes I_n) \right)^\dagger \approx \sum_{\rho=1}^{r_K} (M_{q,\rho} \otimes M_{n,\rho}), \quad \text{where} \quad M_{\ell,\rho} \in \mathbb{R}^{\ell \times \ell}$$

and where \dagger denotes the Moore–Penrose pseudoinverse (see [1], [7, Section 5.2.2]) and r_K is low (i.e., comparable with the Kronecker-rank of the original matrix, i.e., in the 2D case $r_K \lesssim 2$); for related discussion see [28], [12].

Recall the eigenvalue decompositions of L_ℓ s (see Lemmas 3.1–3.4). Notice that all these matrices are positive semi-definite, i.e., their eigenvalues are nonnegative. If we normalize all the eigenvectors of L_ℓ , then the decomposition (3.4) represent the singular value decomposition (SVD) of L_ℓ ,

$$(4.5) \quad L_\ell = V_\ell \Lambda_\ell V_\ell^\top, \quad V_\ell^{-1} = V_\ell^\top.$$

Now, since the right-hand side $H \in \mathbb{R}^{n \times q}$ is in general dense matrix without any particular structure explicitly exploitable for compression, we need to be able to

store several such matrices (i.e., of $\sim nq$ entries) to proceed the PCG algorithm. Thus, if $n \sim q$, then also $n^2 \sim q^2 \sim nq$, and then we are also able to store the full eigendecompositions/SVDs of all L_ℓ s. Moreover, we know these decompositions analytically.¹

Consequently, we have all the important components for the eigendecomposition/SVD of the big matrix L_{2D} (3.5),

$$\left((I_q \otimes L_n) + (L_q \otimes I_n) \right) = (V_q \otimes V_n) \left((I_q \otimes \Lambda_n) + (\Lambda_q \otimes I_n) \right) (V_q \otimes V_n)^\top,$$

and also for its pseudoinverse

$$(4.6) \quad \left((I_q \otimes L_n) + (L_q \otimes I_n) \right)^\dagger = (V_q \otimes V_n) \left((I_q \otimes \Lambda_n) + (\Lambda_q \otimes I_n) \right)^\dagger (V_q \otimes V_n)^\top.$$

The only thing that remains is to calculate low-Kronecker-rank approximation of the matrix in the middle. This matrix is however diagonal

$$\left((I_q \otimes \Lambda_n) + (\Lambda_q \otimes I_n) \right) = \text{diag}(\dots, \lambda_i(L_n) + \lambda_j(L_q), \dots),$$

thus its pseudoinverse takes form

$$\left((I_q \otimes \Lambda_n) + (\Lambda_q \otimes I_n) \right)^\dagger = \text{diag}(\dots, g_{i,j}, \dots), \quad \text{where} \quad g_{i,j} = \begin{cases} \frac{1}{\lambda_i(L_n) + \lambda_j(L_q)} & , \\ 0 & \end{cases}$$

i.e., the nonzero diagonal entries are inverted, the zeros are left as they are. Notice that in practical implementation we consider all the diagonal entries with modulus smaller than 10^{-13} to be zero, thus we replace these entries by zeros in the pseudoinverse.

Now we use similar approach as in previous Section 4.3.1. The inverse of diagonal Kronecker-structured matrix D_ω (4.3) can be written as the Hadamard inverse of (4.4). Thus,

$$(4.7) \quad \widehat{G} = \begin{bmatrix} g_{1,1} & \dots & g_{1,q} \\ \vdots & \ddots & \vdots \\ g_{n,1} & \dots & g_{n,q} \end{bmatrix} = \begin{bmatrix} \lambda_1(L_n) + \lambda_1(L_q) & \dots & \lambda_1(L_n) + \lambda_q(L_q) \\ \vdots & \ddots & \vdots \\ \lambda_n(L_n) + \lambda_1(L_q) & \dots & \lambda_n(L_n) + \lambda_q(L_q) \end{bmatrix}^{\circ\dagger},$$

where \circ^\dagger is the Hadamard (entry-wise) pseudoinverse.

The remaining steps are rather straightforward. To get the best Kronecker-rank r_K approximation of pseudoinverse of the original diagonal matrix, we need to compute

¹However it seems, that the eigendecompositions computed in MATLAB by `eig` function works better than the decompositions assembled entry-wise by using Lemmas 3.1-3.4. Better means the yielding a smaller Frobenius norm $\|L_\ell - V_\ell \Lambda_\ell V_\ell^\top\|_F$.

the best rank r_K (in the standard sense) approximation of \widehat{G} . This can be obtained by using the SVD of \widehat{G} , and employing the Eckart–Young–Mirsky theorem [3], [21]. Let

$$\widehat{G} = X\Sigma Y^\top = \sum_{\rho=1}^{\min(n,d)} x_\rho \sigma_\rho y_\rho^\top$$

be the SVD and its the dyadic expansion. The first r_K dyads, i.e., outer products $x_\rho \sigma_\rho y_\rho^\top$ corresponding to largest singular values can be easily reshaped to Kronecker products of diagonal matrices, e.g., as $\text{diag}(x_\rho \sigma_\rho) \otimes \text{diag}(y_\rho)$. This gives us

$$\begin{aligned} L_{2D}^\dagger &= \left((I_q \otimes L_n) + (L_q \otimes I_n) \right)^\dagger \approx (V_q \otimes V_n) \left(\sum_{\rho=1}^{r_K} \text{diag}(x_\rho \sigma_\rho) \otimes \text{diag}(y_\rho) \right) (V_q \otimes V_n)^\top \\ &= \sum_{\rho=1}^{r_K} \underbrace{\left(V_q \text{diag}(x_\rho \sigma_\rho) V_q^\top \right)}_{M_{q,\rho}} \otimes \underbrace{\left(V_n \text{diag}(y_\rho) V_n^\top \right)}_{M_{n,\rho}}, \end{aligned}$$

the wanted approximation.

We do not provide the algorithmic description of implementation of this preconditioner here, for several reasons. The *first* of them may be more-or-less obvious: If we are able to compute, store, and apply the whole matrix $\widehat{G} \in \mathbb{R}^{n \times q}$ — and we are, because we are able to compute all the matrices Λ_ℓ , to store several matrices of $\sim nq$ entries, and its application is done simply by the Hadamard product, as in Section 4.3.1 — we do not need to approximate this matrix by anything, nor by low-rank object. The low-Kronecker-rank approach seems to be superfluous, it does not work as good as full Kronecker-rank, with about the same cost; see the next Section 4.3.3. The *second* related reason: Initialization of this preconditioner is almost identical to the next one (see Algorithm 4); here we need to extra precompute the SVD of \widehat{G} and prepare matrices $M_{n,\rho}$, $M_{q,\rho}$. Application of this preconditioner (see lines 5 and 14 of Algorithm 1) is almost identical to the application of Laplacian, since both have the same structure, in particular

$$Z_s = \mathfrak{M}_{\text{low-rank}(r_K)}(R_s) = \sum_{\rho=1}^{r_K} M_{n,\rho} R_s M_{q,\rho}^\top.$$

The *third* reason is less obvious: There is no simple generalization of this approach to the 3D case. The low-rank approximation of $\widehat{G} \in \mathbb{R}^{n \times q \times t}$ needs to be done by some kind of high-order SVD (HOSVD), typically the Tucker decomposition (see [24], [25], [26]) or the CP (CanDeComp [2] + ParaFac [8]) decomposition; see also [11]. Tucker decomposition provides optimal approximation, however, the so-called Tucker-core — an analogy of the Σ matrix from the SVD — is not diagonal, but in general full. Thus the total number of the Kronecker summands grows rapidly (cubic in comparison to the SVD in the 2D case). On the other hand, CP decomposition provides

diagonal core tensor and triadic (in general polyadic) decomposition similarly as the SVD, however, the so-called polyadic rank which is involved here, is not well posed due to the lack of orthogonality among individual triads. The *fourth*, the last but not least reason is the positive semi-definiteness of $\mathfrak{M}_{\text{low-rank}(r_{\kappa})}$. Its eigenvalues are entries of the partial sum $\sum_{\rho=1}^{r_{\kappa}} x_{\rho} \sigma_{\rho} y_{\rho}^{\top}$. Since vectors x_{ρ} are mutually orthonormal, and y_{ρ} as well, there is no way (except for $r_{\kappa} = 1$ and $r_{\kappa} = \min(n, q)$) to guarantee these entries to be nonnegative.

4.3.3. *Preconditioning by Moore–Penrose pseudoinverse.* As already indicated in the previous section, to get all necessary components the Moore–Penrose pseudoinverse of $(-\Delta_{\text{FD}})$, we only need to compute the eigendecompositions/SVDs of individual small matrices L_{ℓ} (4.5), which is manageable, and then calculate the Hadamard pseudoinverse of the matrix/tensor of all sums of all eigenvalues of different L_{ℓ} s (4.7). Recall that we consider all the sums with modulus smaller than 10^{-13} to be zero in practical implementation. This is all we need to initialize this preconditioner; see also Algorithms 4 and 5.

Algorithm 4 Initialization of preconditioner $\mathfrak{M}_{\text{p-inv}}$, 2D case

```

1: Input  $L_n, L_q$  {1D Laplacians}
2:  $[V_n, \lambda_1(L_n), \dots, \lambda_n(L_n)] \leftarrow \mathbf{eig}(L_n)$ 
3:  $[V_q, \lambda_1(L_q), \dots, \lambda_q(L_q)] \leftarrow \mathbf{eig}(L_q)$ 
4: For  $i \leftarrow 1, 2, \dots, n$  and  $j \leftarrow 1, 2, \dots, q$ 
5:    $\widehat{G}_{i,j} \leftarrow (\lambda_i(L_n) + \lambda_j(L_q))^{\dagger}$  {threshold for nonzeros:  $10^{-13}$ }
6: End for
7: Output  $V_n, V_q, \widehat{G}$  {eigenvectors, pseudoinverse of sums of eigenvalues}

```

Algorithm 5 Initialization of preconditioner $\mathfrak{M}_{\text{p-inv}}$, 3D case

```

1: Input  $L_n, L_q, L_t$  {1D Laplacians}
2:  $[V_n, \lambda_1(L_n), \dots, \lambda_n(L_n)] \leftarrow \mathbf{eig}(L_n)$ 
3:  $[V_q, \lambda_1(L_q), \dots, \lambda_q(L_q)] \leftarrow \mathbf{eig}(L_q)$ 
4:  $[V_t, \lambda_1(L_t), \dots, \lambda_t(L_t)] \leftarrow \mathbf{eig}(L_t)$ 
5: For  $i \leftarrow 1, 2, \dots, n$  and  $j \leftarrow 1, 2, \dots, q$  and  $k \leftarrow 1, 2, \dots, t$ 
6:    $\widehat{G}_{i,j,k} \leftarrow (\lambda_i(L_n) + \lambda_j(L_q) + \lambda_k(L_t))^{\dagger}$  {threshold for nonzeros:  $10^{-13}$ }
7: End for
8: Output  $V_n, V_q, V_t, \widehat{G}$  {eigenvectors, pseudoinverse of sums of eigenvalues}

```

Application of this preconditioner can be easily understood from the structure of pseudoinverse (4.6). We take the updated residual, transform it into eigenvector-bases, then divide by sums eigenvalues (multiply by their pseudoinverses), and transform back; see also Algorithms 6 and 7.

Algorithm 6 Application of preconditioner $Z_s \leftarrow \mathfrak{M}_{\text{p-inv}}(R_s)$, 2D case

- 1: **Precomputed** V_n, V_q, \widehat{G}
 - 2: **Input** R_s {updated residual}
 - 3: $F_1 \leftarrow V_n^\top R_s V_q$
 - 4: $F_2 \leftarrow F_1 \odot \widehat{G}$
 - 5: $F_3 \leftarrow V_n F_2 V_q^\top$
 - 6: **Output** $Z_s \leftarrow F_3$ {preconditioned residual}
-

Algorithm 7 Application of preconditioner $Z_s \leftarrow \mathfrak{M}_{\text{p-inv}}(\mathcal{R}_s)$, 3D case

- 1: **Precomputed** $V_n, V_q, V_t, \widehat{G}$
 - 2: **Input** \mathcal{R}_s {updated residual}
 - 3: $\mathcal{F}_1 \leftarrow (V_n^\top, V_q^\top, V_t^\top | \mathcal{R}_s)$
 - 4: $\mathcal{F}_2 \leftarrow \mathcal{F}_1 \odot \widehat{G}$
 - 5: $\mathcal{F}_3 \leftarrow (V_n, V_q, V_t | \mathcal{F}_2)$
 - 6: **Output** $Z_s \leftarrow \mathcal{F}_3$ {preconditioned residual}
-

Table 2 summarizes computational cost of this preconditioner while complementing Table 1. We see, that the cost of the pseudoinverse preconditioner is comparable with the ‘full’ (i.e., not the sparse variant) PCG itself. Cost of the eigendecomposition of symmetric matrix of order n is about n^3 , moreover, we deal with matrices (3.1) that are either banded — even tridiagonal (with the exception of the case with periodic BC), or Toeplitz (with the exception of the cases with Neumann BC), so the cost can be further reduced; see [7, Chapter 8], [22], [23]. If we employ the analytic formulas given in Lemmas 3.1–3.4, we can reduce it to about n^2 .

TABLE 2. Cost of the matrix (2D) and tensor (3D) variants of the Moore–Penrose pseudoinverse preconditioner for PCG. The **eigs** may be assembled directly, or computed by an dedicated solver.

	Initialization (Algs. 4, 5)	Application (Algs. 6, 7)
Cost of 2D variant	Cost of 2 eigs + $2nq$	$4nq(n + q + \frac{1}{4})$
Cost of 3D variant	Cost of 3 eigs + $3nqt$	$4nqt(n + q + t + \frac{1}{4})$

Remark 4.3. First it is worth to see once more the lines 3–5 in Algorithms 6 and 7. Columns of $V_\ell s$, i.e., eigenvectors of $L_\ell s$ are sines and cosines (see Lemmas 3.1–3.4). Their outer products, i.e., the eigenvectors of $(-\Delta_{\text{FD}})$, are products of two or three goniometric functions in two or three variables, respectively. Line 3 can be then seen as a kind of expansion of the updated residual into a Fourier series. After division of individual components by the respective eigenvalues in line 4, the preconditioned residual is obtained as a linear combination of these goniometric functions in line 5. Thus, the pseudoinverse preconditioner is in our case essentially a Fourier solver.

Further, the Moore–Penrose pseudoinverse (i.e., in the regular case the inverse) preconditioner can be used in principal as a complete stand-alone direct solver. However, since our matrices might be singular (or close to singular), we need to introduce the threshold (see, e.g., line 5 in 4) which complicates direct application of such direct solver. Therefore, we decided to enclose it into outer loop of PCG. Such two-stage algorithm is not significantly slower since most parts of the pseudoinverse is computed once. On the other hand, one can anticipate, that such preconditioning causes rapid convergence of the outer PCG.

5. NUMERICAL RESULTS

We present here several selected experiments we performed on data corresponding to three different testing problems. More realistic results can be found in already published paper in Physical Review B [15] that is partially based on the presented approach.

5.1. Testing problems. The first problem tests basic scalability, it consists of four right-hand side matrices, or better to say, four discretizations of the same continuous right-hand side. The second problem contains only one right-hand side matrix and its purpose is to test different boundary conditions. The third problem consists of four a bit more realistic right-hand sides — it deals with random distribution of charge and three of the right-hand sides are 3D. Thus, we present here in total nine testing right-hand sides (six 2D and three 3D). All of these right-hand sides are artificially fabricated by FERRODO2; see [16], [15].

Problem 5.1 (Regular two-periodic problem). *The first sample is a 2D problem, with regular alternating diagonal lines (or narrow stripes) of positive and negative charges; see Figure 1 (indices in the images are shifted by one compared to matrices, and start at 0). This problem is periodic in both physical dimensions, i.e., the corresponding Laplacian is singular. We work with four discretizations of the same right-hand side, from the coarsest to the finest: 5×10 , 20×40 , 50×100 , and 500×1000 .*

Problem 5.2 (Problem with mixed boundary conditions). *The second problem is also 2D, positive charge is localized in a single band; see Figure 2. On the left we prescribe zero electric potential, i.e., Dirichlet condition $u_L = 0$, whereas on the right its derivative, i.e., the Newton condition $e_R = -\frac{1}{2}$. In the vertical direction, the problem is periodic. We use only one discretization of moderate size 40×120 .*

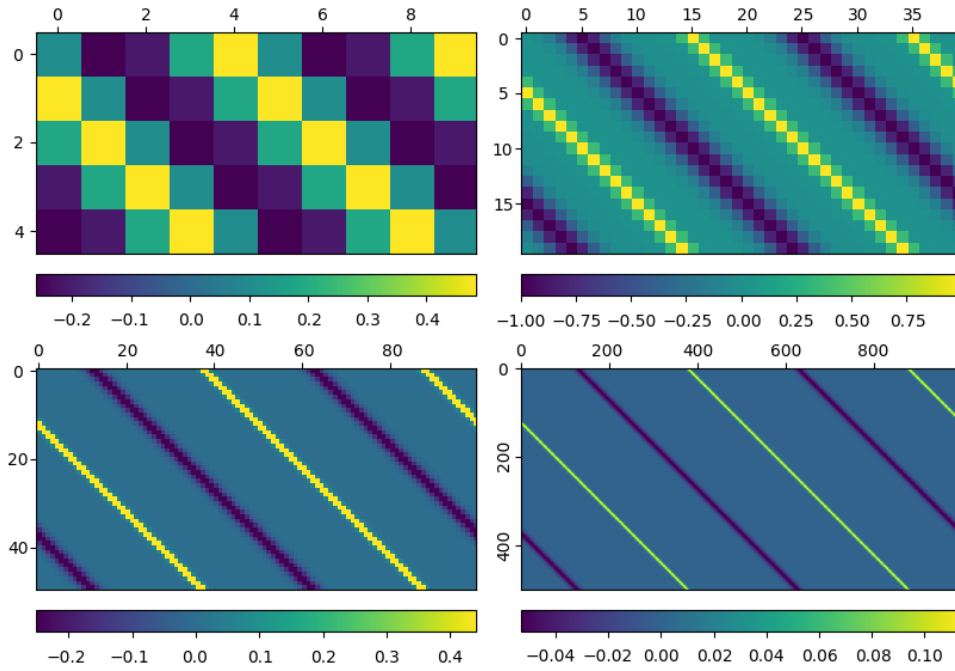


FIGURE 1. Four right-hand sides of the regular two-periodic problem (see Problem 5.1).

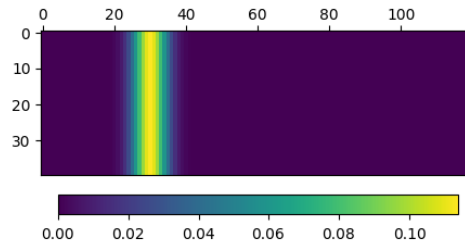


FIGURE 2. Right-hand side of the problem with mixed boundary conditions (see Problem 5.2).

Problem 5.3 (Problem with randomly distributed localized charge). *The last problem is little bit more realistic. It is again periodic in all physical dimensions (so the Laplacian is singular; similarly as in Problem 5.1), the charge is localized in two stripes, but randomly distributed; these stripes are not the same, the positive charge spreads in wider strip than the negative. This problem consists of four right-hand sides: the first one is 2D 512×256 , the remaining three are 3D $128 \times 64 \times 8$, $128 \times 64 \times 64$, and $512 \times 256 \times 8$. Figure 3 shows the first frontal slice in the case of 3D data (all slices look similarly).*

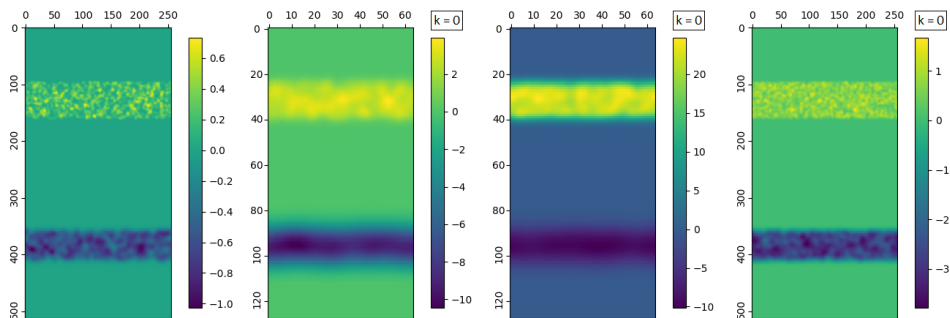


FIGURE 3. Four right-hand sides of problem with randomly distributed charge (see Problem 5.3). Notice that strips are of different width — negative charge is more localized. The last three images show the first frontal slices ($k = 0$) of three-way tensors.

5.2. Numerical experiments. In all experiments we started the PCG with zero initial guess, i.e., $U_0 = 0_{n,q}$ in 2D, or $\mathcal{U}_0 = 0_{n,q,t}$ in 3D cases. All the problems, in particular the right-hand sides (and thus also the initial residuals) are for convenience and better comparability of the results normalized such that

$$(5.1) \quad \|H\|_F = \|\text{vec}(H)\|_2 = \frac{1}{nq} = \|R_0\|_F \quad \text{and} \quad \|\mathcal{H}\| \equiv \|\text{vec}(\mathcal{H})\|_2 = \frac{1}{nqt} = \|\mathcal{R}_0\|,$$

in the respective cases. In all the following plots we measure the effectiveness of individual methods (preconditioners) by the real run-time of the PCG. To obtain reasonable results:

- First we experimentally fix the number of iterations for each pair of problem and preconditioner, to get true residual small enough (we are not interested in stopping criterion at this moment; see Remark 4.2).

- Then we run the method several times (usually ten-times) and calculate the average run-time. We measure the time for the initialization and the time for the iterative part separately.
- Since the cost of individual iteration is independent on the iteration number, we compute the time for one iteration simply by further averaging (the average time for the iterative part over total number of iterations).

These times are affected by collecting all the data during the PCG run, however, we collect the same data of the same size in each iteration for each preconditioner. Presented results are computed by: MATLAB R2024a (version 24.1.0.2653294, update 5) running at Microsoft Windows 10 Pro (version 10.0, build 19045, 64 bit), Dell Latitude 5410 with Intel Core i5-10310U CPU @ 1.70/2.21 GHz and 8 GB RAM.

Experiment 5.4 (Justification of method and convergence metric choices). *The first experiment is rather formalistic. We employ the second finest right-hand side of Problem 5.1, i.e., we solve linear system with 5000 unknowns.*

Since we already mentioned the Jacobi-like stationary iteration scheme in Section 4.3.1, we use it there for preconditioning, but we can use it as a stand-alone method. Figure 4 compares convergence of the unpreconditioned CG and Jacobi-like method for three different values of ω . One can easily see the dominance of CG. Notice that the (horizontal) time axis is in logarithmic scale, due to disproportional run-times of both methods. Notice also that we need more than 6500 of Jacobi iterations to converge, thus we mark only each 250th.

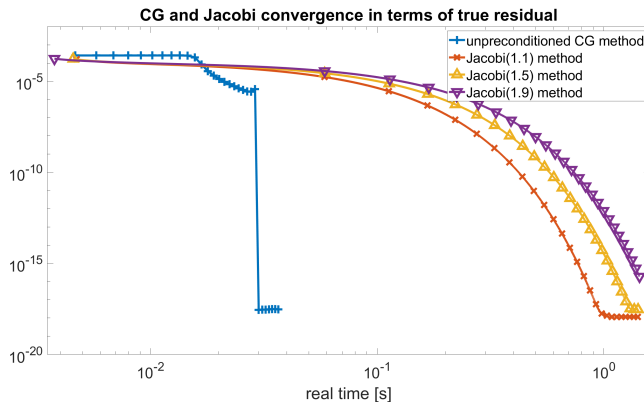


FIGURE 4. Convergence of unpreconditioned CG and Jacobi-like stationary iterative method for different values of ω . Time axis is in logarithmic scale; markers at convergence curves for Jacobi denotes each 250th iterations (see Experiment 5.4).

We measure the convergence by the norm of the true residual (i.e., $\|h - Lu_s\|_2$ in 1D case). This choice is definitely wrong for CG/PCG (see also Remark 4.2). However in our relatively simple problem of Poisson's equation, it seems to be applicable. Figure 5 shows behavior of the true residual and the computed residual (i.e., norm $\sqrt{\rho_s} = \|r_s\|$ from Algorithm 1) — both quantities are indistinguishable up to the moment of convergence, then the true residual stagnates while computed further decrease; see, e.g., [18] or [13]. We also plotted quantity that behaves like the L -norm of error. By the L -norm of error we understand (again in 1D case, for simplicity)

$$\|u_s - u\|_L = \sqrt{(u_s - u)^\top L (u_s - u)} = \sqrt{u_s^\top Lu_s - 2u_s^\top Lu + u^\top Lu} \geq 0.$$

Since u is the exact solution, then $Lu = h$. Thus

$$\|u_s - u\|_L^2 = \underbrace{u_s^\top Lu_s - 2u_s^\top h}_{\kappa_s} + \|u\|_L^2 \geq 0,$$

where the underbraced part κ_s is fully computable, and (the square of) the L -norm of u is unknown, but constant. Thus we compute all κ_s s, shift them to get nonnegative quantities, e.g., $\kappa_s - \min_s(\kappa_s)$, and square-root them; altogether we approximate

$$\|u_s - u\|_L \approx \eta_s \equiv \sqrt{\kappa_s - \min_s(\kappa_s)} \geq 0.$$

The final quantity η_s is in the plot further scaled and shifted for better comparability with the residuals; we plot in particular

$$\alpha \eta_s + \beta, \quad \text{where} \quad \alpha = \frac{\|h - Lu_1\|_2}{\eta_1}, \quad \text{and} \quad \beta = \varepsilon_M = 2^{-52} \approx 2.2204 \cdot 10^{-16}$$

is the machine precision. Our goal not to get robust approximation, but to observe possible drops in the norm. Figure 5 shows that the most significant drop in all of the three mentioned descriptors (both residuals and L -norm of error approximation) coincides. Notice that we complement this information by fourth descriptor: Since we use problem with singular matrix, we also observe the norm of the null-space component in the solution. In all the remaining plots we restrict ourselves only to the true residual.

Experiment 5.5 (Performance of various preconditioners). In the second experiment we again use the second finest right-hand side of Problem 5.1. We compare PCG with individual preconditioners, each with some basic settings. In particular: $\mathfrak{M} = I$ (no preconditioner), $\mathfrak{M}_{\text{Jacobi}(3,1.3)}$ (three steps of Jacobi-like method, i.e.,

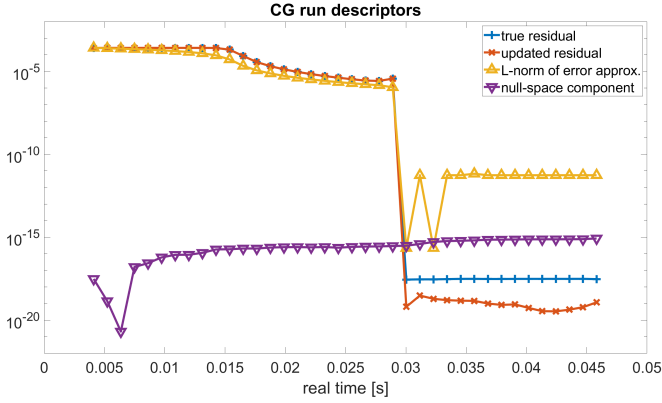


FIGURE 5. Behavior of unpreconditioned CG observed by several quantities (see Experiment 5.4).

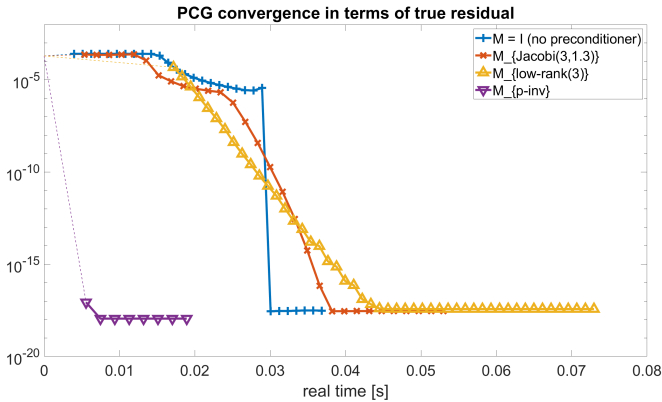


FIGURE 6. PCG with various preconditioners applied on Problem 5.1 of size 50×100 (see Experiment 5.5).

$p = 3$, with $\omega = 1.3$), $\mathfrak{M}_{\text{low-rank}(3)}$ (Kronecker rank $r_K = 3$ approximate inverse), and $\mathfrak{M}_{\text{p-inv}}$ (pseudoinverse preconditioner).

We see that the unpreconditioned CG starts fastest as expected. On the other hand, the slowest start has the PCG with low-Kronecker-rank preconditioner, as already discussed in the last paragraph of Section 4.3.2. Its convergence is very straightforward, however slower than for unpreconditioned CG. Nevertheless, PCG with the Moore–Penrose pseudoinverse-based preconditioner beats them all — its convergence is very rapid. After the first iteration it is already almost done (we use

the almost inverse for preconditioning), however the second iteration further pushes down the true residual.

For completeness, Figures 7 and 8 illustrate behavior of parametrized preconditioners $\mathfrak{M}_{\text{Jacobi}(p,\omega)}$ and $\mathfrak{M}_{\text{low-rank}(r_K)}$, respectively. One can see that the low-Kronecker-rank preconditioner is getting closer to the pseudoinverse preconditioner with higher rank, but with more expensive initialization. The artifact on the already converged curve for r_K is probably due to the indefiniteness of the preconditioner (which was indicated for $r_K = 4$ and 7).

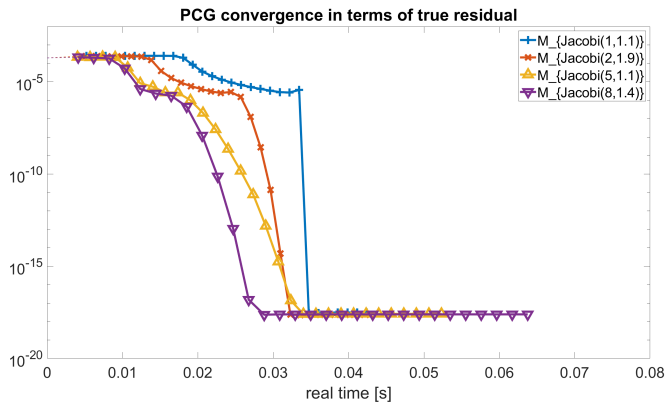


FIGURE 7. Performance of Jacobi-like preconditioner is only weakly involved by the number of inner iterations p or the value of the splitting parameter ω (compare with Figure 6).

Experiment 5.6. The third experiment is to verify the performance of the chosen preconditioner — the pseudoinverse-based — on all three testing problems, all nine right-hand sides. For the results see Figure 9.

Notice that the first and smallest system is of 50 equations, whereas the largest is of 1 048 576 equations. PCG for such systems converge on disproportional time-scales. To make the results visible in one plot, the time axis needs to be also in logarithmic scale. Therefore, we cannot start the curve at zero time; thus the convergence curves start at the time after initialization and show only the iterative part. This brings another problem: Since the convergence is very rapid, already in the first iteration, and initial part is missing, we cannot directly see from where it converges whereto. Recall that the norm of the initial residual is normalized (5.1); i.e., $\|R_0\|_F = 2 \cdot 10^{-2}$ for the smallest, and $\|\mathcal{R}_0\| = 9.5367431640625 \cdot 10^{-7}$ for the largest system.

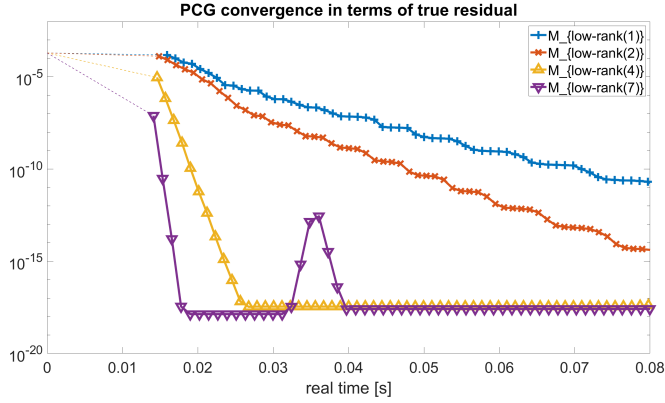


FIGURE 8. Low-Kronecker-rank approximation of inverse works as preconditioner significantly better with higher ranks r_K (if it works, see the last paragraph of Section 4.3.2; compare with Figure 6).

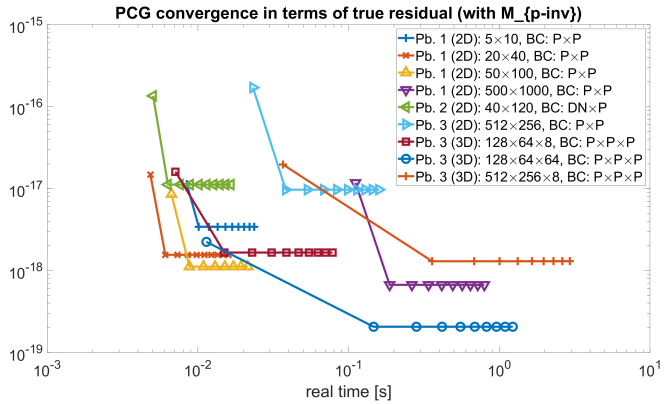


FIGURE 9. The convergence curve of PCG with the pseudoinverse-based preconditioner is almost problem independent. Time axis is in logarithmic scale (see Experiment 5.6).

5.3. **Solutions.** Just for completeness we present the approximate solutions of all three problems, computed by PCG with pseudoinverse-based preconditioner, in Figure 10. Since in Problem 5.1 (the top plot) the charge is localized in thin parallel and equidistant lines, the electric potential changes linearly between these lines. In the solution of Problem 5.2 (the middle plot) the electric potential is fixed on the left edge at zero and on the right it falls down with the rate $-1/2$, as prescribed by the boundary conditions. The unequal width of two stripes with randomly distributed

charges in Problem 5.3 (the bottom plot) causes different curvature of the electric potential.

6. CONCLUSIONS

We have presented an implementation of the preconditioned method of conjugate gradient (CG) that is suitable for Kronecker-structured problems. In our case particularly the Poisson’s problem originated in ferroelectricity. We have briefly analyzed several preconditioners, their behavior and also computational cost in comparison to the CG itself.

Since the right-hand side is dense with general rank(s) (thus we cannot exploit its low-rank structure and employ the low-rank arithmetic) and of shape close enough to square (or cube, or hyper-cube), we are in principle able to store also the individual objects of the Kronecker-structured system operator in dense format. Consequently, we were able to reasonably well approximate the Moore–Penrose pseudoinverse of the operator, and use this approximation for preconditioning of CG.

This way preconditioned CG converges rapidly. So rapidly that only a few iterations is necessary — in our case of a simple Laplace operator, it seems that two or three are sufficient (but we perform ten, to be sure; see Figure 9). Perhaps, instead of a *CG with pseudoinverse-based preconditioner*, it would be better to call this approach a *pseudoinverse-based direct solver with refinement by CG-iteration*.

The presented implementation is done in MATLAB and serves mostly for testing of methods and preconditioners. We prepared also C/C++ version that employs the Intel oneAPI Math Kernel Library (MKL); see [30], [31]. This version is implemented into, and practically used in the code FERRODO2; see [16], [15]. First results computed by this code have been already published in Physical Review B [15].

ACKNOWLEDGEMENTS

We wish to thank to Jana Žáková for her help with preparation of the manuscript of this paper.

REFERENCES

- [1] *A. Ben-Israel, T. N. E. Greville: Generalized Inverses: Theory and Applications* (2nd ed.). Springer, New York, 2003. Zbl 1026.15004, DOI 10.1007/b97366
- [2] *J. D. Carroll, J. Chang: Analysis of individual differences in multidimensional scaling via an n -way generalization of “Eckart–Young” decomposition*, *Psychometrika*. 35 (3) (1970), pp. 283–319. Zbl 0202.19101, DOI 10.1007/BF02310791
- [3] *C. Eckart, G. Young: The approximation of one matrix by another of lower rank*, *Psychometrika*, 1 (1936), pp. 211–218. Zbl 62.1075.02
- [4] *L. C. Evans: Partial differential equations* (2nd ed.), *Graduate Studies in Mathematics Volume 19*, American Mathematical Society, Providence, 2010. Zbl 1194.35001, DOI 10.1090/gsm/019

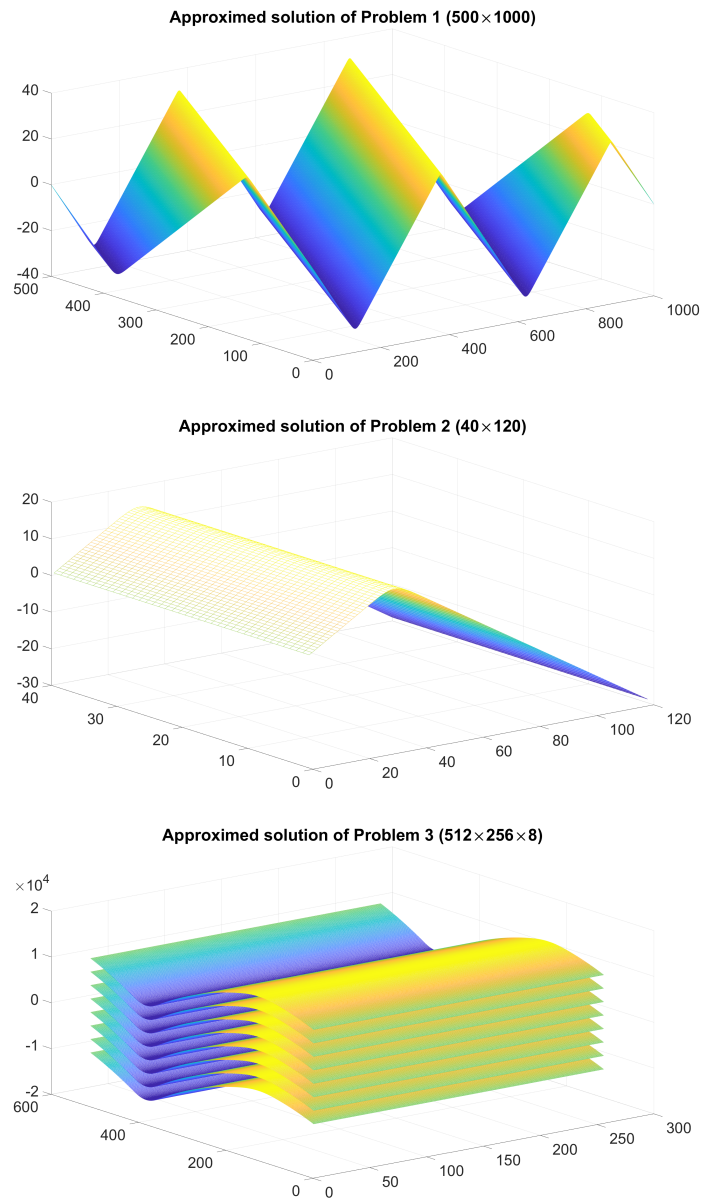


FIGURE 10. Approximate solutions of all three problems. Vertical axis measures the electric potential (in the bottom plot, there is the vertical scale related to the fifth layer from the top).

- [5] *R. P. Feynman*: Feynman lectures on physics. Vol. 2, Mainly electromagnetism and matter, Addison-Wesley, Reading, 1964.
- [6] *M. Fiedler*: Special matrices and their applications in numerical mathematics (2nd ed.), Dover Publications, Dover, 2008. Zbl 1170.65018
- [7] *G. H. Golub, C. F. Van Loan*: Matrix computations (4th ed.), Johns Hopkins University Press, Batimore, 2013. Zbl 1268.65037
- [8] *R. A. Harshman, Richard* Foundations of the PARAFAC procedure: Models and conditions for an “explanatory” multi-modal factor analysis, UCLA Working Papers in Phonetics 16, 1970.
- [9] *M. R. Hestenes, E. Stiefel*: Methods of conjugate gradients for solving linear systems, Journal of Research of the National Bureau of Standards 49(6) (1952), pp. 409–436. Zbl 0048.09901, DOI 10.6028/jres.049.044
- [10] *J. Kolářová*: Spectral properties of discretized Laplace operator (in Czech), Diploma thesis, Technical University of Liberec, 2024. URL <https://stag.tul.cz/StagPortletsJSR168/CleanUrl?urlid=prohlizeni-prace-detail&praceIdno=47663>.
- [11] *T. G. Kolda, B. W. Bader*: Tensor decompositions and applications, SIAM Review 51(3) (2009), pp. 455–500. Zbl 1173.65029, DOI 10.1137/07070111X
- [12] *D. Kressner, M. Plešinger, C. Tobler*, A preconditioned low-rank CG method for parameter-dependent Lyapunov matrix equations, Numerical Linear Algebra with Applications 21(5) (2014), pp. 666–684. Zbl 1340.65077, DOI 10.1002/nla.1919
- [13] *J. Liesen, Z. Strakoš*: Krylov subspace methods: Principles and analysis, Oxford University Press, Oxford, 2012. Zbl 1307.65001, DOI 10.1093/acprof:oso/9780199655410.001.0001
- [14] *J. Málek, Z. Strakoš*: Preconditioning and the conjugate gradient method in the context of solving PDEs, SIAM Spotlights 1, Philidelphia, 2015. Zbl 1396.65002, DOI 10.1137/1.9781611973846
- [15] *P. Marton, M. A. P. Gonçalves, M. Paściak, S. Körbel, V. Chumchal, M. Plešinger, A. Klíč, J. Hlinka*: Zigzag charged domain walls in ferroelectric PbTiO₃, Physical Review B 107(9) (2023), paper id 094102, pp. 1–9. DOI 10.1103/PhysRevB.107.094102
- [16] *P. Marton, J. Hlinka*: Simulation of domain patterns in BaTiO₃, Phase Transitions 79(6–7) (2006), pp. 467–483. DOI 10.1080/01411590600892351
- [17] *J. C. Maxwell*: A dynamical theory of the electromagnetic field, Philosophical Transactions of the Royal Society of London 155 (1865), pp. 459–512. DOI 10.1098/rstl.1865.0008
- [18] *G. Meurant*: The Lanczos and conjugate gradient algorithms: From theory to finite precision computations, SIAM Software, Environments, and Tools 19, Philadelphia, 2006. Zbl 1110.65029, DOI 10.1137/1.9780898718140
- [19] *G. Meurant, J. Papež, P. Tichý*: Accurate error estimation in CG, Numerical Algorithms 88(3) (2021), pp. 1337–1359. Zbl 1490.65056, DOI 10.1007/s11075-021-01078-w
- [20] *G. Meurant, P. Tichý*: Error norm estimation in the conjugate gradient algorithm, SIAM Spotlights 6, Philidelphia, 2024. Zbl 07851831, DOI 10.1137/1.9781611977868
- [21] *L. Mirsky*: Symmetric gauge functions and unitarily invariant norms, The Quarterly Journal of Mathematics, Oxford Second Series, 11 (1960), pp. 50–59. Zbl 0105.01101, DOI 10.1093/qmath/11.1.50
- [22] *B. N. Parlett*: The symmetric eigenvalue problem (unabridged, corrected republication of 1980), SIAM Classics in Applied Mathematics 20, Philidelphia, 1998. Zbl 0885.65039, DOI 10.1137/1.9781611971163
- [23] *Y. Saad*: Numerical methods for large eigenvalue problems (revised ed.) SIAM Classics in Applied Mathematics 66, Philidelphia, 2011. Zbl 1242.65068, DOI 10.1137/1.9781611970739
- [24] *L. R. Tucker*: Implications of factor analysis of three-way matrices for measurement of change, Problems in Measuring Change (C. W. Harries ed.), University of Wisconsin Press, Madison, WI, 1963, pp. 122–137.
- [25] *L. R. Tucker*: The extension of factor analysis to three-dimensional matrices, in: Contributions to Mathematical Psychology (H. Gulliksen and N. HoltFrederiksen eds.), Holt, Rinehardt & Winston, New York, 1964, pp. 110–127.

- [26] *L. R. Tucker*: Some mathematical notes on three-mode factor analysis, *Psychometrika*, 31 (1966), pp. 279–311, DOI 10.1007/BF02289464
- [27] *D. A. Turkington*: Generalized vectorization, cross-products, and matrix calculus, Cambridge University Press, Cambridge, 2013. Zbl 1307.15001, DOI 10.1017/CBO9781139424400
- [28] *E. Ullmann*: A Kronecker product preconditioner for stochastic Galerkin finite element discretization, *SIAM Journal on Scientific Computing*, 32 (2010), pp. 923–946. Zbl 1210.35306, DOI 10.1137/080742853
- [29] *R. S. Varga*: Matrix iterative analysis (2nd revised and expanded ed.), Springer, Berlin, 2000. Zbl 0998.65505, DOI 10.1007/978-3-642-05156-2
- [30] *E. Wang, Q. Zhang, B. Shen, G. Zhang, X. Lu, Q. Wu, Y. Wang*: Intel Math Kernel Library, in: High-Performance Computing on the Intel[®] Xeon Phi[™], Springer, Cham, 2014, pp. 167–188. DOI 10.1007/978-3-319-06486-4_7
- [31] Intel[®] oneAPI Math Kernel Library (oneMKL). URL <https://www.intel.com/content/www/us/en/developer/tools/oneapi/onemkl.html>.

Authors' addresses: *Věnceslav Chumchal*, Department of Mathematics, Technical University of Liberec, Studentská 1402/2, 461 17 Liberec 1, Czech Republic, e-mail: venceslav.chumchal@tul.cz & venceslav.chumchal@gmail.com. *Pavel Marton*, Institute of Physics, Czech Academy of Sciences, Na Slovance 2, 182 00 Praha 8, Czech Republic, & Institute of Mechatronics and Computer Engineering, Technical University of Liberec, Studentská 1402/2, 461 17 Liberec, Czech Republic, e-mail: pavel.marton@tul.cz. *Martin Plešinger* (corresponding author), Department of Mathematics, Technical University of Liberec, Studentská 1402/2, 461 17 Liberec 1, Czech Republic, e-mail: martin.plesinger@tul.cz. *Martina Šimůnková*, Department of Mathematics, Technical University of Liberec, Studentská 1402/2, 461 17 Liberec 1, Czech Republic, e-mail: martina.simunkova@tul.cz.